Bistatic Ultra-wideband SAR For Imaging Of Ground Targets Under Foliage

Lars M.H. Ulander. Ph.D., Swedish Defence Research Agency (FOI)
Torleif Martin, Ph.D., Swedish Defence Research Agency (FOI)

Key Words: SAR, Ultra-wideband, Bistatic, FOPEN, FDTD

SUMMARY & CONCLUSIONS

Bistatic SAR is compared with monostatic SAR concerning, e.g. coherent integration time and spatial resolution. We also suggest that bistatic SAR may be used to suppress background clutter, e.g. when the clutter scattering is dominated by dihedral or trihedral scattering mechanisms. This idea is applied to the problem of detecting concealed vehicles in foliage using VHF-band SAR. Electromagnetic simulations show that the vehicle-to-clutter ratio can dramatically increase by choosing different incidence angles for the transmitter and receiver in a bistatic SAR.

1. *INTRODUCTION*

Long-range air-to-ground surveillance of stationary and moving targets requires synthetic-aperture radar (SAR) with ground moving target indication (GMTI). Both modes use coherent signal processing to achieve its capabilities. The SAR mode generates high-resolution images independent of the distance between the radar and the ground, whereas the GMTI mode performs target detection and positioning by using multiple antenna phase centres in combination with space-time signal processing techniques.

Despite its unique capabilities, a SAR/GMTI system has several tactical shortcomings. Firstly, the threat from counter measures is high since the emitted electromagnetic energy may be intercepted. Secondly, SAR data is collected along an extended flight track which introduces a time delay (coherent integration time) between the first and last radar echoes from the target which need to be processed in order to obtain full image resolution. In fact, the integration time may be several minutes for high-resolution imaging using long-range systems.

There is currently a strong interest in investigating alternative radar concepts which may circumvent the above-mentioned shortcomings. One such concept which we discuss in this paper is bistatic radar [1], i.e. with physically separated transmitter and receiver. The transmitter is preferably positioned at large distance in order to minimise the probability of interception, whereas the receiver is close to the target in order to reduce integration time [2].

The objective of the present paper is to investigate the implications of such an imaging system. Geometric resolution in monostatic SAR is well-understood [3] but this is not the case for bistatic SAR. In the paper, we propose a model for bistatic image resolution and illustrate its usefulness for assessing different bistatic geometries [2]. Finally, we investigate the potential of bistatic SAR for detecting targets concealed in foliage by numerical electromagnetic simulations.

.

2. *BISTATIC GROUND SURVEILLANCE RADAR SYSTEM*

The basic idea of introducing a bistatic ground surveillance radar system is to move the transmitting platform (illuminator) far away from hostile territory. Longer distance directly translates into a reduced threat level for the platform and thus a higher chance of survival. The receiving platforms (receptors), on the other hand, may operate at closer range since they are only passive sensors. The receptors may also employ signature reduction technology in order to avoid being detected.

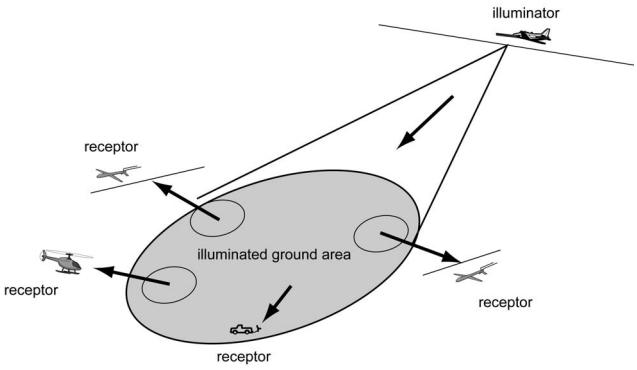

Figure 1. Example bistatic ground surveillance system with one illuminator and four receptors.

The update rate for a long-range high-resolution and monostatic SAR is of the order of minutes. However, for a bistatic SAR the integration time can be much shorter if the receiver is positioned close to the target area. The tables below show typical integration times for two example monostatic and bistatic SAR systems.

Table 1. Integration time for two monostatic SAR systems.

Frequency	Range	Velocity	Resolution	Int. time
X-band	200 km	300 m/s	0.1 m	100 s
VHF-band	55 km	300 m/s	3 m	200 s

Table 2. Integration time for two bistatic SAR systems

Frequency	Range	Velocity	Resolution	Int. time
X-band	1 km	300 m/s	0.1 m	1 s
VHF-band	1 km	300 m/s	3 m	6 s

We conclude that the integration time may be significantly shorter in a bistatic SAR and at the same time reduce the threat against the transmitting platform.

3. *BISTATIC SAR SPATIAL RESOLUTION*

One of the most important properties of an imaging system is its spatial resolution. A linear imaging system is uniquely characterized by its impulse response function or, after Fourier transformation, the system transfer function. The frequency domain support of the transfer function is important since it determines the finest possible spatial resolution corresponding to the diffraction limit.

The bistatic SAR geometry is shown in Figure 2. One platform transmits a pulse signal and the other platform receives a delayed echo scattered off ground objects. The distance between the transmitting platform and the scatterer is denoted R_T, whereas the distance between the scatterer and the receiving platform is denoted R_R. The position vectors to the transmission platform, the receiving platform and the scatterer are denoted by $\boldsymbol{r_T}$, $\boldsymbol{r_R}$ and $\boldsymbol{r}$, respectively.

In the following, we assume that the "start-stop-approximation" is valid, i.e. that the platforms are "frozen" during pulse propagation. In other words, the platforms are assumed to stop during transmission and reception and then move on to the next position. It can be shown to be a good approximation also for moving platforms since the speed of light is much larger than the platform velocities. In the case that the start-stop-approximation is not valid, corrections may be included to take into account the finite speed of light.

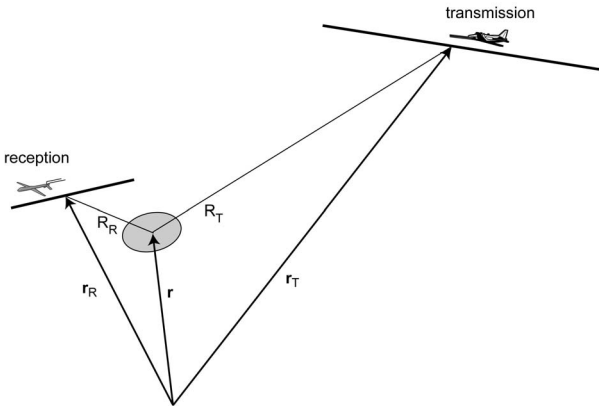

Figure 2. Bistatic SAR imaging geometry. The scattering object is assumed to be located at $\boldsymbol{r}$, the illuminator (transmission) at $\boldsymbol{r_T}$, and the receptor (reception) at $\boldsymbol{r_R}$.

We assume a linear propagation medium which is isotropic, homogeneous and non-dispersive, i.e. the speed of light c is constant in space. The ground is also assumed to be a collection of single-scattering objects (Born approximation) so that superposition applies. The received signal from a point object at $\boldsymbol{r} = \boldsymbol{r}'$ is therefore given by

$$g(s,t) = \frac{p\left(t - \dfrac{2R(s,\boldsymbol{r}')}{c}\right)}{R(s,\boldsymbol{r}')} \tag{1}$$

where $p(t)$ is the pulse signal after compression. The received signal is expressed as a function of "slow time" s and "fast time" t, where the latter corresponds to time delay from transmission and the former is the time which defines the platform positions. The "range" $R(s,\boldsymbol{r})$ in (1) is defined according to

$$R(s,\boldsymbol{r}) = \frac{|\boldsymbol{r} - \boldsymbol{r_T}(s)| + |\boldsymbol{r_R}(s) - \boldsymbol{r}|}{2} \tag{2}$$

The amplitude scaling in (1) should really be $1/R^2$ according to the radar equation but has here been chosen to $1/R$ in order to simplify the derivations. It is not a critical issue since any range dependence can be compensated in the signal processing provided that the compressed pulse is short.

SAR inversion assuming point-like scattering objects is obtained by applying the backprojection principle. This means that the received pulse echoes are backprojected and accumulated to all possible positions from which scattering may have occurred. That is, an image $h(\boldsymbol{r})$ is formed according to the following integral transformation

$$h(\boldsymbol{r}) = \int g\left(s, \frac{2R(s,\boldsymbol{r})}{c}\right) ds \tag{3}$$

The aperture integration is performed along the flight track. For each aperture point (slow time) s, the radar data $g(s,t)$ is backprojected and accumulated to all points $\boldsymbol{r}$ for which the time delay t equals $2R(s,\boldsymbol{r})/c$.

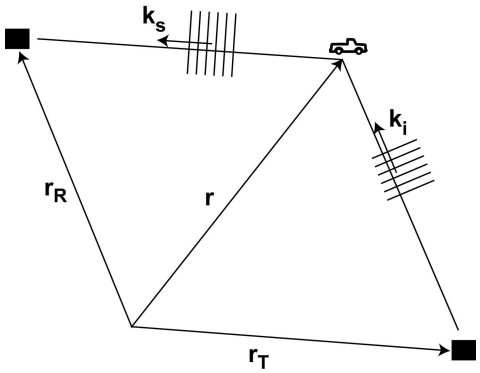

Figure 3. A bistatic radar illuminates the object with wave vector $\boldsymbol{k_i}$ and receives the scattered field with wave vector $\boldsymbol{k_s}$.

Consider now the bistatic image response in the vicinity of a point object which is located at a large distance from both antennas as illustrated in Figure 3. This assumption is

equivalent to a plane-wave approximation and (2) can be simplified according to

$$R(s,\boldsymbol{r}) \approx \frac{(\boldsymbol{k}_i - \boldsymbol{k}_s)\cdot \boldsymbol{r} + \boldsymbol{k}_s \cdot \boldsymbol{r}_R - \boldsymbol{k}_i \cdot \boldsymbol{r}_T}{2k} \quad (4)$$

Inserting (4) into (1) and (3) leads to

$$h(\boldsymbol{r}) \approx \int \frac{p\left((\boldsymbol{k}_i - \boldsymbol{k}_s)\cdot(\boldsymbol{r}-\boldsymbol{r}')/\omega\right)}{R(s,\boldsymbol{r}')}\, ds \quad (5)$$

which can be further simplified by noting that R in the denominator varies slowly and can be moved outside the integration. Equation (5) can also be rewritten using the Fourier transform $P(\omega)$ of the pulse $p(t)$ resulting in

$$h(\boldsymbol{r}) \approx \frac{1}{2\pi R}\iint P(\omega)\exp\left[j(\boldsymbol{k}_i(s)-\boldsymbol{k}_s(s))\cdot(\boldsymbol{r}-\boldsymbol{r}')\right] ds\, d\omega \quad (6)$$

Fourier transformation of (6) gives the transfer function

$$H(\boldsymbol{k}) \approx \frac{\exp[-j\boldsymbol{k}\cdot\boldsymbol{r}']}{2\pi R}\iint P(\omega)\, F(\boldsymbol{k},s)\, ds d\omega \quad (7)$$

where

$$F(\boldsymbol{k},s) = \iiint \exp\left[-j(\boldsymbol{k}-\boldsymbol{k}_i(s)+\boldsymbol{k}_s(s))\cdot\boldsymbol{r}\right] dxdydz \quad (8)$$

is non-zero only for $\boldsymbol{k} = \boldsymbol{k}_i(s) - \boldsymbol{k}_s(s)$. Equations (7) and (8) show that the image spectrum $H(\boldsymbol{k})$ has a support in spatial frequency domain defined by the variation of the vector $\boldsymbol{k}_i(s) - \boldsymbol{k}_s(s)$ over aperture positions s and frequencies ω. For all other points, the image spectrum is close to zero.

We apply this model for two cases: A monostatic SAR with a straight flight track and a bistatic SAR with the transmitter located at a large distance and the low-flying receiver located close to the imaged area.

The first case is a monostatic SAR, for which the two vectors $\boldsymbol{k}_i(s)$ and $-\boldsymbol{k}_s(s)$ are parallel and hence $\boldsymbol{k} = 2\boldsymbol{k}_i(s)$. The vector $\boldsymbol{k}$ rotates an angle $\Delta\vartheta$ when the antenna moves along the synthetic aperture as illustrated in Figure 4. It also scales in magnitude over the frequency band so that the frequency domain support is defined within the grey-shaded area Ω in Figure 4. The minimum resolution area in the slant range plane is thus given by [1]

$$\Delta A \geq \frac{(2\pi)^2}{\Omega} = \frac{\lambda_c}{2\Delta\vartheta}\frac{c}{2B} \quad (9)$$

where λ_c is the wavelength corresponding to the centre frequency.

The second case is a bistatic SAR, for which the vector $\boldsymbol{k}_i(s)$ is constant and the vector $-\boldsymbol{k}_s(s)$ rotates $\Delta\vartheta$ as shown in Figure 5. The minimum area resolution can be shown to be given by

$$\Delta A \geq \frac{2\lambda_c}{(\Delta\vartheta + \cos\vartheta_1 - \cos\vartheta_2)}\frac{c}{2B} = \frac{2\lambda_c}{[\Delta\vartheta + 2\sin(\Delta\vartheta/2)]}\frac{c}{2B} \quad (10)$$

where the last equality is only valid for a symmetric aperture angle, i.e. $\vartheta_{1,2} = 90^o \pm \Delta\vartheta/2$. Comparing (9) and (10), we conclude that a bistatic radar requires approximately twice the aperture angle compared to a monostatic radar in order to achieve the same spatial resolution.

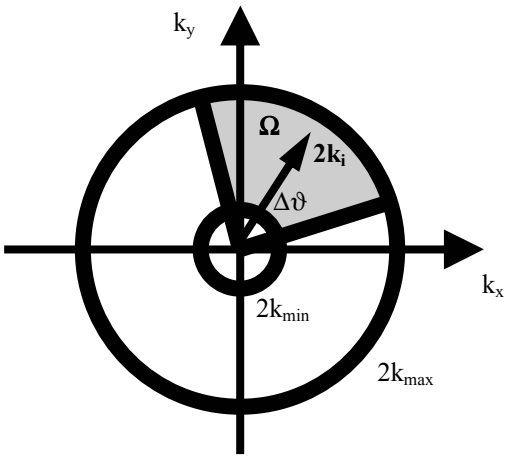

Figure 4. Frequency support for a monostatic SAR image.

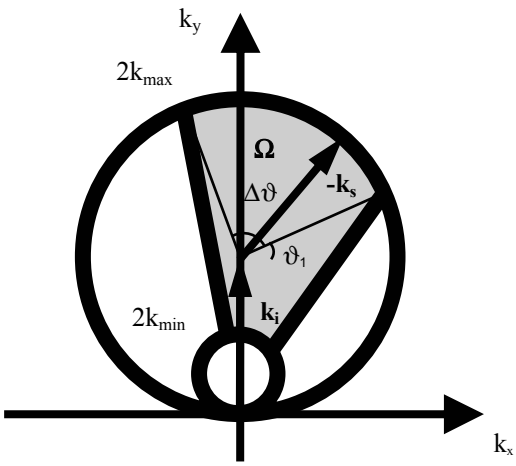

Figure 5. Frequency domain support for a bistatic SAR image. One of the platforms provides a constant wave vector $\boldsymbol{k}_i$ and the other platform provides a wave vector $\boldsymbol{k}_s$.

.

4. *ELECTROMAGNETIC SIMULATIONS*

A bistatic SAR may, in some cases, have a significant advantage in terms of clutter suppression. This is the case

when the clutter signal is dominated by a strong dihedral or trihedral scattering mechanism. One such example is the use of VHF-band SAR for foliage penetration (FOPEN), i.e. the problem of detecting vehicles in foliage concealment. The monostatic VHF-band clutter is most often dominated by dihedral scattering from the tree stem and the ground. This is dominating when the angle between the trees and ground are close to 90º. However, a bistatic SAR with sufficiently large difference in incidence angle between the transmit and receive antennas will experience a significant reduction since the scattering will move out of the strong dihedral scattering lobe. The scattering from the vehicle is also often dominated by a dihedral-like scattering mechanism formed between the target and the ground. However, the reduction in radar cross section for a vehicle is found to be much smaller since the target is much lower than a normal tree. This effect opens up a possibility of dramatically improving the vehicle-to-clutter-ratio by using a bistatic SAR configuration.

Numerical scattering simulations of targets in the open and under foliage cover have been performed using an FDTD code developed at FOI [4] which includes interaction with the ground modeled by a dielectric half volume. Signatures have primarily been studied in the 20-90 MHz band corresponding to the frequency band used by the CARABAS airborne SAR developed at FOI [5].

Forest stands are modeled using the results of individual tree simulations, since numerical experiments have shown that multiple scattering effects between trees are negligible. An example of a tree model is shown in Figure 6 for a 15 meter spruce tree modelled with an FDTD grid resolution of $D_x = D_y = 5$ cm and $D_z = 7$ cm. Although this resolution is relatively high, yielding a large computational volume, convergence studies for vehicles have shown that the required resolution for a maximum error of 2 dB in a SAR image is surprisingly low. FDTD cell sizes of 15 cm – 20 cm are often sufficient in this case, despite that the minimum wavelength is 3 m in free space and approximately 1 m in the ground. An example of a FDTD simulation is shown in Figure 7.

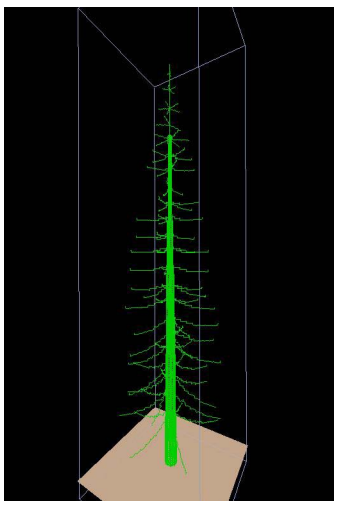

Figure 6. Geometry of the 15-m high spruce tree used for electromagnetic simulations in the low VHF-band.

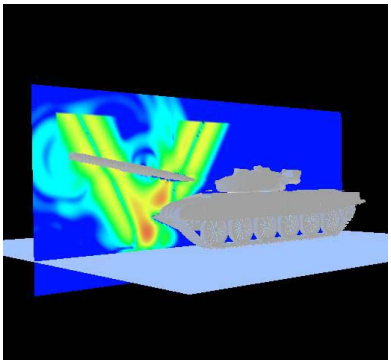

Figure 7. A snapshot from a FDTD simulation when a plane wave is incident on a T72 tank. The pulse is a derivative Gaussian pulse which which gives broadband scattering results at each incident angle along a flight path.

The simulation results of individual vehicles and trees have been combined in a SAR simulator where both monostatic and bistatic scenarios can be investigated. A monostatic result at incidence angle 65° is shown in Figure 8 with six identical military terrain vehicles (TGB11) at different positions in the open and under foliage cover. The ground projected SAR image is shown together with the vehicle and tree models. Note that the tree models are simplified in this 3D view (the real electromagnetic simulation models are of the same type as the one shown in Figure 6). A corresponding bistatic result is shown in Figure 9, where the (fixed) transmitted plane wave is incident at 80° and the receiving platform is at an incidence angle of 65°. Comparing the two SAR images in Figure 8 and Figure 9, we conclude that the vehicle-to-clutter ratio is dramatically increased in the bistatic case (typically 15 dB). Note that the color coding scheme of the mono- and bistatic SAR images are different and that the vehicle radar-cross sections are in fact rather similar.

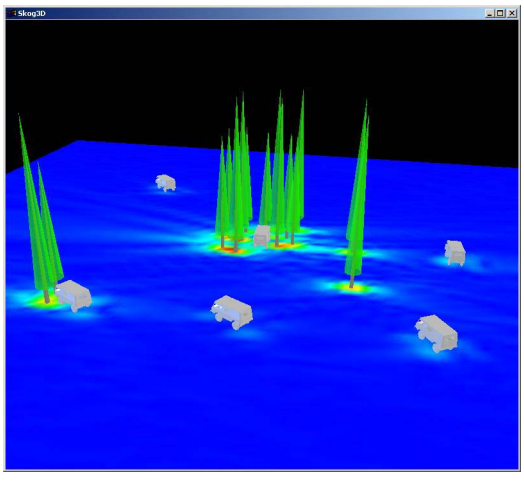

Figure 8. FDTD simulation of a monostatic 20-90 MHz SAR imaging six vehicles and a number of trees. The object models are projected onto the resulting color-coded SAR image.

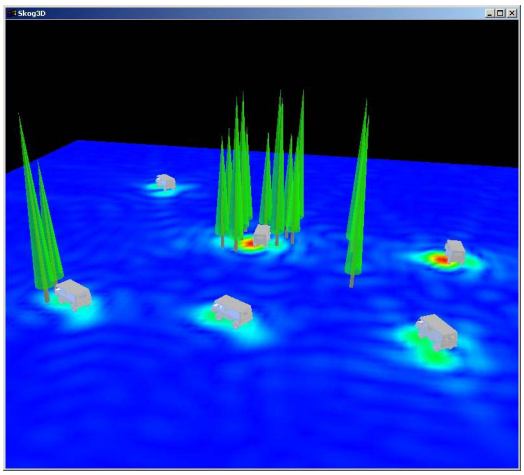

Figure 9. FDTD simulation of a bistatic 20-90 MHz SAR imaging the same scene as in Figure 8. However, note that the color-coding of the SAR image is different in order to more clearly show the reduction in the tree radar-cross section.

5. *CONCLUSIONS*

Bistatic SAR has been investigated and compared with monostatic SAR. We conclude that integration time can be made significantly shorter in a bistatic SAR by placing the (passive) receiver close to the imaged area, whereas the transmitter can be moved back to longer ranges resulting in lower threat levels. We have derived a new model for bistatic SAR spatial resolution. It is noted that approximately twice the aperture angle is need for a bistatic SAR in order to achieve the same resolution as a monostatic SAR. We have also proposed that bistatic SAR may be used to suppress clutter, e.g. when the clutter scattering is dominated by dihedral or trihedral scattering mechanisms. This idea has been applied to the problem of detecting concealed vehicles in foliage. Electromagnetic simulations show that the vehicle-to-clutter ratio can dramatically improve by choosing different incidence angles for the transmitter and receiver.

REFERENCES

1. N.J. Willis, "Bistatic Radar", Artech House, 1991.
2. L.M.H. Ulander, "Theoretical Considerations of Bi- and Multistatic SAR", FOI Report FOI-R--1334--SE, 2004.
3. L.M.H. Ulander, and H. Hellsten, "A New Formula for SAR Spatial Resolution", *AEÜ (International Journal of Electronics and Communications)*, Vol. 50, No. 2, pp. 117-121, 1996.
4. T. Martin, and L.M.H. Ulander, "Bistatic SAR Pilot Study: Simulations using FDTD", FOI Report FOI-R--0839--SE, 2003
5. H. Hellsten, L.M.H. Ulander, A. Gustavsson, and B. Larsson, "Development of VHF CARABAS II SAR", *Proceedings SPIE Conference on Radar Sensor Technology*, Orlando, Fl., 8-9 April 1996, SPIE Vol. 2747, pp. 48-60, 1996

BIOGRAPHIES

Lars M.H. Ulander was born in Växjö, Sweden, on Dec 5, 1962. He received the M.Sc. in 1985 and the Ph.D. in 1991, both from Chalmers University of Technology (CTH) in Gothenburg, Sweden.

He joined the Swedish Defence Research Agency (FOI) in 1995 to work on airborne VHF-band synthetic-aperture radar (SAR). His research focuses on signal processing techniques for VHF- and UHF-band SAR systems, as well as implementing and evaluating such techniques in airborne demonstrators such as the CARABAS and LORA systems developed at FOI. He is currently Director of Research at FOI in Radar Signal Processing. He is also Adjunct Professor in Radar Remote Sensing at CTH since 1999.

He is the author or co-author of more than 150 professional publications of which more than 30 in refereed journals. He is the holder of four patents, and is listed in *Who's Who in Electromagnetics.*